


Beyond the phase stability in standard Stark decelerationQing Liu,¹ Wenli Li,¹ Shanwu Wang,¹ Chenyue Pan,² Du Wang,³ Tao Yang,^{1,4,5} Dongdong Zhang ⁶,
Shunyong Hou,^{1,*} and Jianping Yin¹¹*State Key Laboratory of Precision Spectroscopy, East China Normal University, Shanghai 200062, China*²*China World Academy, Changshu, Jiangsu 215500, China*³*Shanghai Starriver Bilingual School, Shanghai 201108, China*⁴*Xinjiang Astronomical Observatory, Chinese Academy of Sciences, Urumqi, Xinjiang 830011, China*⁵*Collaborative Innovation Center of Extreme Optics, Shanxi University, Taiyuan, Shanxi 030006, China*⁶*Institute of Atomic and Molecular Physics, Jilin University, Changchun 130012, China*

(Received 8 September 2024; revised 4 January 2025; accepted 3 March 2025; published 24 March 2025)

Improving the number and number density of cold molecules is a longstanding goal in cold molecule research. Stark deceleration provides an important access to taming polar molecules and makes the collision and high-resolution spectroscopy a reality. However, the full deceleration efficiency of the traditional Stark decelerator has been impeded by its intrinsic loss mechanisms, which significantly limit its applications. In this paper, we introduce an interspersed guiding deceleration strategy that surpasses the periodic phase stability limitations of traditional Stark decelerator. Our approach is theoretically and experimentally validated using the ND₃ molecule, achieving significant gains of 3 ~ 8 for all final velocity ranges. Additionally, our method requires a lower operation number of switching that is beneficial for reducing the consumption of the high-voltage switches and suitable for controlling a large number of deceleration stages. This method is applicable to any traditional crossed-pin Stark decelerator and can stop a wider variety of molecular species with higher densities, including those with a small Stark shift-to-mass ratio. It is anticipated to become an essential tool for producing cold and dense molecular samples, offering promising prospects for cold collision studies and precision measurements.

DOI: [10.1103/PhysRevA.111.032816](https://doi.org/10.1103/PhysRevA.111.032816)**I. INTRODUCTION**

Thanks to its unique advantages such as long interaction range and anisotropy, cold gas-phase polar molecules have attracted keen interest from physicists and chemists, showing extensive applications ranging from cold molecular collisions [1–4] to precision measurements [5–7]. Following the pioneering work of Stern and Gerlach in the 1920s [8], it has been established that the motion of particles (either atoms or molecules) can be manipulated using external fields. Twenty-five years ago, the advent of Stark deceleration for polar molecules signified a breakthrough in achieving comprehensive three-dimensional (3D) motion control over neutral molecular beams [9], thereby facilitating the preparation of translationally cold (<1 K) molecules within the laboratory's coordinate system. Although several methods, including Rydberg-Stark deceleration [10], laser cooling [11,12] and buffer gas cooling [13,14], have been developed to generate cold molecules, Stark deceleration and its magnetic counterpart Zeeman deceleration [15,16] stand out as a specialized and efficient technique for taming polar (paramagnetic) molecular beams. This beam deceleration method yields cold molecular samples characterized by high density, pure state, and controllable velocity. This technique not only bridges the gap between supersonic molecular beams and cold molecular samples but also connects to other control manners such as electric/magnetic traps [17–21], storage

rings [22], and synchrotrons [23,24]. Through Stark deceleration, a variety of polar molecules have been successfully stopped [25–27]. This advancement opens up opportunities for precision measurements [6,7,28,29], cold collision studies [3,30,31], and quantum computing science [32,33].

Stark deceleration typically begins with a supersonic beam, which is produced by adiabatic expansion and exhibits properties of being internally cold yet possessing rapid translational speed (300 m/s–2000 m/s, depending on the carrier gas). Note that this is the only cooling process for the Stark deceleration technique, since the densities of molecular packets within the Stark decelerator are too low to facilitate thermalization. Consequently, the concept of temperature utilized in this context merely serves as a convenient representation of the molecular velocity distribution. The Stark decelerator operates by repeatedly (e.g., 100 times) switching on and off inhomogeneous, time-varying electric fields to reduce the velocity of a subset of molecules within the supersonic beam that are in a specific quantum state. Ideally, these molecules could be safely transported to the end of the decelerator without any loss. However, traditional Stark decelerators (i.e., pulsed crossed-pin electrodes) experience significant molecular loss due to inherent loss mechanisms [34,35]. It is noteworthy that a higher number or increased density of molecules often facilitates unlocking the full potential of molecular sample studies mentioned above. For Stark deceleration, there are two strategies to achieve this objective. One strategy involves enhancing the number density of the molecular beam before it enters the Stark decelerator, such as creating a denser supersonic beam using faster pulsed valves [36], or utilizing a frozen skimmer

*Contact author: syhou@lps.ecnu.edu.cn

[37,38] to improve the quality of the supersonic beam. Another approach is to boost the deceleration efficiency, which is precisely the focus of this paper.

Over the past two decades, significant efforts have been devoted to addressing the intractable problems of standard Stark decelerators. These efforts can be roughly divided into three categories. The first category involves modifying the operating time sequence for switching the electrodes, such as using a so-called $S = 3$ mode [34,39,40], advanced switching [41], focusing operation [42] or multiphase methods [43–45]. Using this method, the deceleration can be improved by a factor of 2 to 6 and even more [46] compared to the traditional operation method. The second approach is to modify the structure of the decelerator, like quadrupole-guiding decelerators [34] where a quadrupole-guiding stage is interleaved between each deceleration stage. Gains of 5 and 40% can be expected for intermediate velocity ($v_{\text{final}} > 80$ m/s) and low final velocity ($v_{\text{final}} = 14$ m/s), respectively. The last approach involves ring-shaped Stark decelerators, including switched ring Stark decelerators [47,48] and traveling wave Stark decelerators [49–54]. This method enables generating true 3D potential wells to avoid losses that occur in traditional Stark decelerators. It usually allows for producing moderately strong electric fields, making it more favorable for decelerating heavy polar molecules (>100 amu) [51,52,55] whose energy levels usually drop under high electric fields. For a given traditional Stark decelerator, only the first approach is adoptable. In this paper, we will add a new means to the toolbox of the first approach to further improve the deceleration efficiency of traditional Stark decelerators.

Our operation strategy does not need any hardware modification and is easy to implement. It involves using every third stage for guidance instead of deceleration, while the remaining stages are used for deceleration (referred to as the interspersed guiding deceleration operation mode, IGD). By adopting this operation mode, not only is the transverse focus enhanced, but the limit of the coupling between the longitudinal and transverse motions can be effectively circumvented. Significant gains are achieved for all ranges of final velocities. Additionally, the power consumption of the high-voltage (HV) switches is greatly reduced due to the number of switching times being reduced by one-third. This method is readily applicable to existing decelerators and allows for more applications.

II. STANDARD OPERATION ($S = 1$) AND OVERTONE OPERATION ($S = 3$)

The detailed operation principles of a standard Stark decelerator can be found in the literature [9,43], here we only give a brief description. The standard pulsed Stark decelerator is composed by an array of pairs of crossed cylindrical metal rods, which are orthogonal to a beam line that passes between them and enable yielding two kinds of 1D static electric lattice in the longitudinal direction. Figure 1(a) illustrates the distributions of these fields along the z axis, differentiated by solid and dashed lines. These lines correspond to the electric configurations during the activation of the odd and even stages, respectively. Additionally, the precalculated operation time sequences for both stages are presented. In Figs. 1(a)–1(c),

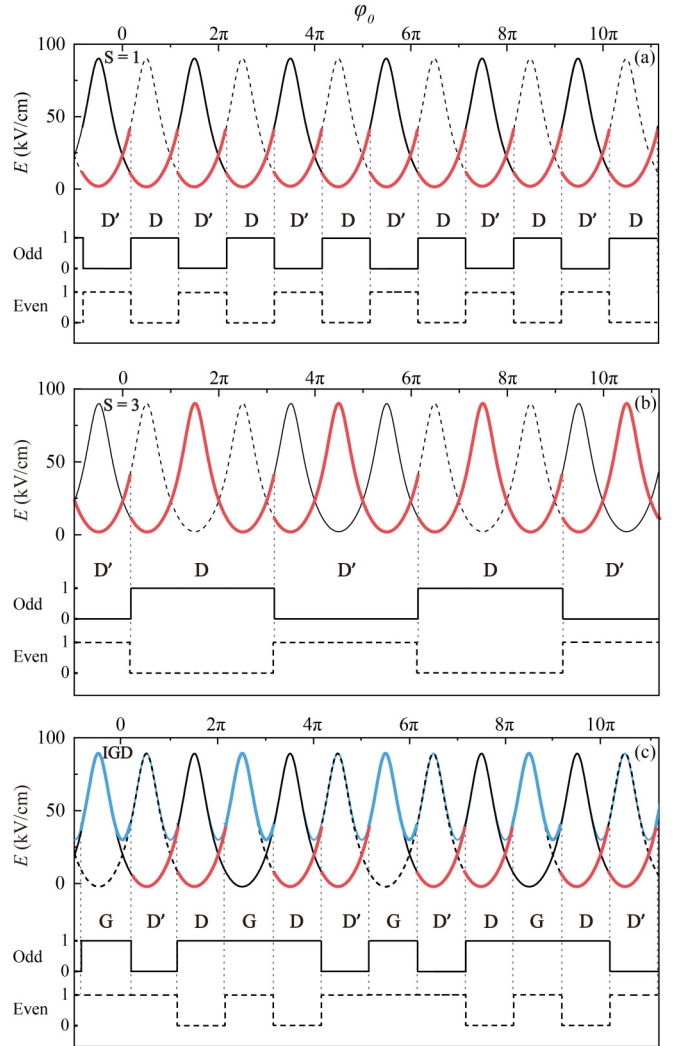


FIG. 1. Diagram of the electric fields experienced by an ideally synchronized molecule in three switching modes for $\varphi_0 = 30^\circ$, i.e., $S = 1$ (a), $S = 3$ (b) and IGD (c). On the upper half of each panel, the thin solid and dashed black lines represent the two electric field configurations used for deceleration, while the thin blue line depicts the guiding electric field configuration. The bold red and blue lines indicate the electric fields traversed by the synchronous molecule. On the lower half of each panel, the solid and dashed lines depict the corresponding time sequences for both odd and even electrode stages, respectively. In (c), the synchronous molecule undergoes a two-stage deceleration process D' and D , followed immediately by a guiding manipulation G .

the bold red and blue lines illustrate the electric fields experienced by the so-called “synchronous molecule”, which refers to the idealized molecule that is always sync with the time sequence and has no transverse velocity. The molecule around the synchronous molecules and populated in the phase space stability area of the decelerator, in principle, can be brought to the end of the decelerator without loss. The area of the phase space stability of the decelerator is strongly dependent on the reduced longitudinal position (i.e., phase angle) φ_0 , where $\varphi_0 = \pi z_0/L$ with z_0 being the longitudinal position of the synchronous molecules and L being the distance

between longitudinally adjacent electrodes. Since the electrodes enable alternately focusing molecules in one transverse direction, and thus their transverse confinement in both transverse directions achieved as they experience more than one stage. Combining the longitudinal phase space area and the transverse confinement of the molecules, it is clear that the decelerator works by alternately switching on/off the two electric field configurations to produce a discretely moving effective 3D Stark potential well to slow down molecules. There are two points that should be stressed. First, the effective 3D potential well is obtained based on time-average transverse and longitudinal forces and it is valid provided that $v_z/L \gg f$, where v_z is the longitudinal velocity of the molecules and f is the oscillation frequency in the traveling trap. If this validity was broken, molecule loss in low-velocity region will occur, such as transverse over focusing and longitudinal reflection [34]. The second issue is transverse-longitudinal coupling, which is attributed from the fact that both the longitudinal and transverse forces are offered by the same electrodes [35]. It gives rise severe molecular loss during deceleration. The simplest way to circumvent this problem is to let the molecules fly through an energized deceleration stage without removing the field. That is to say only part of the deceleration stages are used to decelerate molecules and the remaining are employed for more transverse confinement. This is exactly the overtone operation. Figure 1(b) shows the overtone operation of $S = 3$, where every third electrodes is utilized for deceleration. This operation manner fully reduces the loss of molecules resulted from the transverse-longitudinal coupling [34,39]. However, it comes at the expensive of the decelerator length.

III. INTERSPERSED GUIDING DECELERATION OPERATION (IGD)

The principle of our proposed operation mode is schematically illustrated in Fig. 1(c), where guiding operations are interspersed within the standard $S = 1$ mode, with every third electrode designated for beam guidance and the remaining electrodes for energy removal. As depicted in Fig. 1(c), three electric field configurations will be utilized in the IGD mode, represented by black solid, dashed, and blue solid lines, respectively. The electric field configurations depicted by the solid and dashed lines are employed for deceleration while the field configuration depicted by the blue line is used for transverse guidance. The bold red and blue lines in sections indicate the electric fields traversed by the synchronous molecule. In IGD operation mode, the synchronous molecule undergoes successive deceleration through two stages. At the end of the deceleration phase angle, rather than switching off the field of the activated stages (as in $S = 1$ mode), conjugated electrode pairs are activated, resulting in the simultaneous powering of both odd and even stages (indicated by the blue curve). Once the synchronous molecule has traveled one period, the conjugated electrode pair is switching off again, allowing further deceleration of the synchronous molecule. The effective field experienced by the synchronous molecule exhibits a shape similar to that in the $S = 3$ mode, albeit with significantly reduced guiding length and potential depth. These controls are denoted by the letters D, D', and G, as shown in Fig. 1(c). The switching time sequences for odd and even stages in IGD

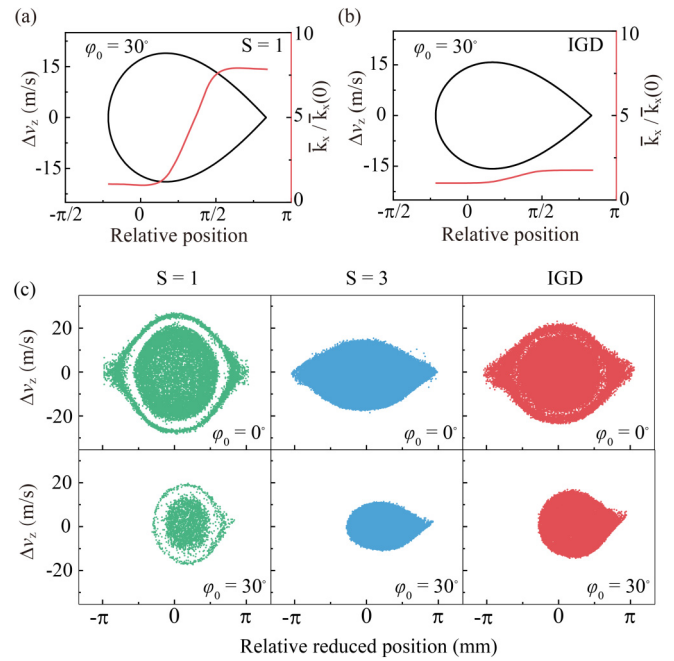


FIG. 2. The longitudinal properties of the Stark decelerator under two operation modes: (a) a standard mode, and (b) an IGD mode. The black lines denote the longitudinal phase space separatrix, while the red lines signify the transverse average spring constants as a function of relative reduced position. The transverse average spring constant is normalized to that experienced by the synchronous particle, denoted as $\bar{k}_x(0)$. (c) Simulated phase space fillings using three distinct operation modes, specifically for two values of ϕ_0 : 0° and 30° .

operation mode are also presented at the bottom of Fig. 1(c). By comparing the time sequences in Figs. 1(a)–1(c), it is observed that in the $S = 1$ mode, the number of switches is equivalent to the number of electrode stages traversed by the synchronous molecule, whereas in $S = 3$ and IGD modes, the number of switches constitutes one third and two thirds of the traversed stages, respectively. The consumption of HV switches is strongly dependent on the switching frequency. During experiments, considerable instantaneous currents and thus a significant amount of heat are produced when HV switches are turned on or off. This heat must be dissipated promptly to prevent performance degradation or damage to the switches. Therefore, IGD operation mode is advantageous for reducing high-voltage switch consumption and is suitable for controlling a large number of deceleration stages.

In Fig. 2, the longitudinal and transverse properties are compared for a standard mode of operation and IGD mode. In both cases, the separatrix in the longitudinal phase space and the average transverse spring constants $\bar{k}_{x,y}(\Delta\phi)$ are depicted. As can be seen in Figs. 2(a) and 2(b), the transverse force in standard operation mode is strongly dependent on the relative position, by contrast, the transverse force does not differ by a factor of 3 within the separatrix in the IGD mode. Figure 2(c) shows the longitudinal phase space distributions via three different operation modes, resulting from 3D trajectory calculations with two different values of phase angles ($\phi_0 = 0^\circ$, $\phi_0 = 30^\circ$). The input parameters for the three operation modes are all the same. For standard mode ($S = 1$), there exist

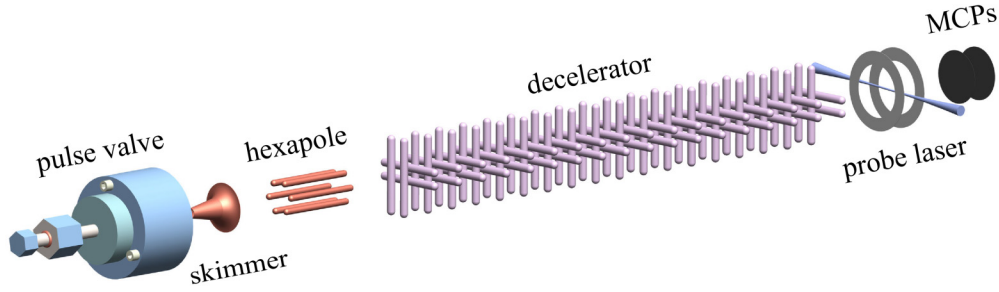


FIG. 3. Schematic of our Stark deceleration setup.

structures in the separatrix for both angles, where molecules are unstable in the empty or sparse areas. In contrast, no structure in the distribution is observed in $S = 3$ operation, while the separatrices are smaller than that of $S = 1$ mode. In the case of the IGD mode, there is a thin halo in the phase space stability areas for $\varphi_0 = 0^\circ$, which is similar to that of the standard mode but with a much denser molecular density in the central region. However, for $\varphi_0 = 30^\circ$ no structure in the distribution is observed.

IV. EXPERIMENTAL DEMONSTRATION

A detailed introduction to the Stark deceleration system in our laboratory was previously provided [56]. Figure 3 schematically illustrates the setup of the Stark deceleration, which is composed of three differentially pumped vacuum chambers. A pulsed supersonic beam is generated by freely expanding a gas mixture of 6% ND_3 (deuterated ammonia) in 1.5 atm xenon through a 0.5-mm-diameter pulsed valve into the source chamber. The valve operates at room temperature (293 K) and opens for a duration of 180 μs . After passing through a 2-mm-diameter skimmer and a 40-mm-long hexapole, the ND_3 molecular beam is then coupled into the Stark decelerator. The decelerator is made up of 180 pairs of 3-mm-diameter cylindrical parallel-placed steel rods, where the center-to-center distance between the two rods in each pair is 5 mm, leaving a 2 mm opening gap in the transverse directions. The adjacent pairs of rods are perpendicular to each other and are separated by a distance of 6 mm, resulting in the total length of the decelerator being 1.08 m. The opposing rods are, respectively, connected to different polarity power supplies via their own HV switches (*Behlke Elektronik HTS 201-03-GSM*). A total of four HV switches and two HV power supplies are required for the decelerator device. The resulting beam from the last slowing stage freely travels a distance of ~ 23 mm to the detection zone and is then ionized by a focused dye laser (~ 317 nm). The resulting ions are detected by a pair of microchannel plates and the signals are recorded by a personal computer. The time sequence used to control the four HV switches is calculated in advance and is consistent with the one used in the numerical simulations. In operation, the pressure in the source chamber and the detection chamber is typically 5×10^{-4} Pa and 5×10^{-6} Pa, respectively.

To accurately assess the deceleration efficiency differences between standard operation mode and IGD, identical initial conditions were used for the following deceleration experiments. The decelerator was operated at voltages of ± 10 kV, generating a maximum electric field on the beam axis

of 90 kV/cm. The ND_3 molecular beam's initial center velocity was approximately 332 m/s with a full width at half maximum velocity spread of 60 m/s. Molecules in the low-field-seeking state $|J, K, M\rangle = |1, 1, -1\rangle$ were selected and decelerated to various final velocities. Figure 4 illustrates the observed final velocity dependence of TOF (time of flight) traces independently using $S = 1$, $S = 3$, and IGD modes. At final velocities exceeding 220 m/s, the molecular signal intensity of $S = 3$ and IGD significantly surpasses that of $S = 1$ operation mode. However, the limited deceleration ability of $S = 3$ mode makes it challenging to produce cold molecular samples with final velocities below 200 m/s in our setup. In contrast, the IGD mode effectively achieves greater gain compared to $S = 1$ mode across all final velocity regions. It is important to note that the IGD mode is not suitable for low final velocities; hence, when the final velocity

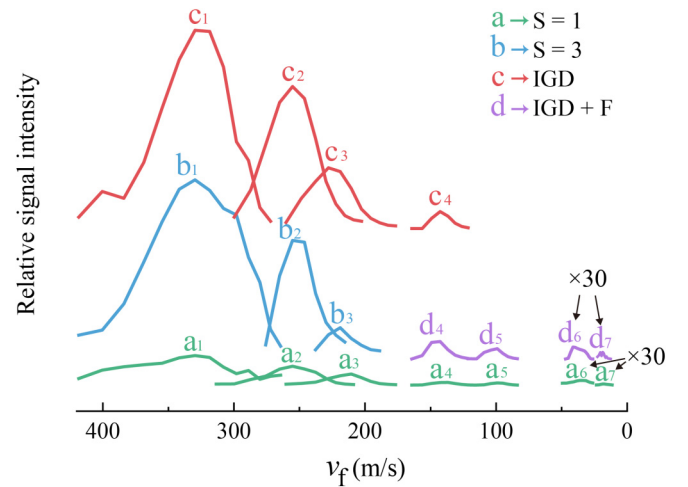


FIG. 4. Comparison of observed TOF profiles using $S = 1$ (lower traces), $S = 3$ (middle traces, front), IGD + F (middle traces, back), and IGD mode (upper traces). The ND_3 beam with the same initial velocity of 332 m/s is tuned to a variety of final velocities, namely, 332 m/s, 260 m/s, 220 m/s, 140 m/s, 100 m/s, 40 m/s and 20 m/s. In $S = 1$ mode, the corresponding phase angles used are as follows: 0° , 15.3° , 22.1° , 31.8° , 34.8° , 37.5° , 37.9° . In $S = 3$ mode, the corresponding phase angles used are 0° , 43° and 61.2° . IGD mode, when the final velocity is above 100 m/s, the corresponding phase angles used are 0° , 22.7° , 32.3° and 45.9° . When the final velocity falls 100 m/s and below, the mode changes to IGD + F, the corresponding phase angles used are 45.6° , 49.9° , 53.1° , and 53.7° . The curves for $S = 3$, IGD + F and IGD have been vertically offset for clarity.

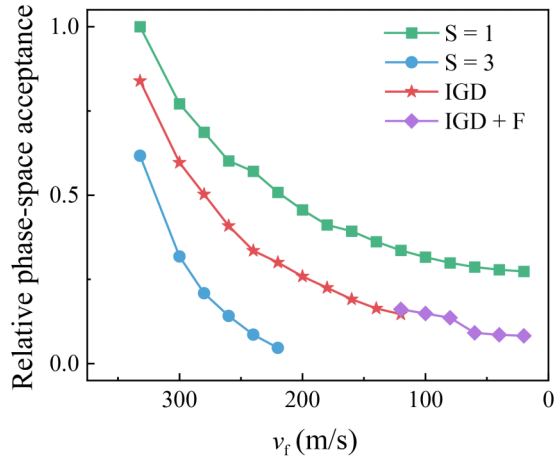


FIG. 5. Calculated stable longitudinal phase area of various modes over a range of final velocities. All data is normalized to the signal peak obtained in $S = 1$ operation mode at $\varphi_0 = 0^\circ$.

falls 100 m/s and below during the deceleration process, the remaining stages switch to focusing operation F as depicted in Fig. 1 of Ref. [42]. Figure 5 depicts the phase space stability region for various operation modes. Although the phase space stability region of $S = 1$ mode is the largest at any final velocity, it yields the smallest number of molecules due to its significant loss mechanism. Packets obtained from the IGD mode have a narrower longitudinal velocity spread, resulting in much colder samples than those produced from the standard mode.

Figure 6 shows the final velocity dependency of the signal density for various operation modes, which are achieved by integrating molecular packets depicted in Fig. 4. It can be observed that the signal intensity of IGD (or IGD + F) is 5 to 8 times stronger than the $S = 1$ mode at speeds exceeding 100 m/s and 3 to 5 times stronger at speeds of 100 m/s and below. Numerical simulations for the experimental results in Fig. 6(a) are depicted in Fig. 6(b). The variation of signal intensity with the final velocity, as obtained through the four

operational modes, matches well with theoretical predictions. However, the simulation predicts that the amplitude should be approximately 2 to 3 times larger than observed in the experiment in the high final velocity regime. This discrepancy is primarily attributed to nonadiabatic losses [57] experienced by the ND_3 molecules. In the Stark deceleration process, a change to any high-field seeking state would result in the molecule being drawn towards the electrodes where the electric field intensity peaks. Such undesired state alterations arise because the molecules experience a time-varying electric field as they move through the decelerator and as the decelerator is switched from one field configuration to another [57]. Given the sizable region where transitions occur and the fact that our deceleration experiment involves 179 field switches in the $S = 1$ mode, a significant fraction of molecules may be driven into another state and lost from the decelerator. However, both the IGD and $S = 3$ operation modes can largely mitigate nonadiabatic losses because their switching times, during which nonadiabatic transitions might occur, are only half and one-third of those in $S = 1$ mode, respectively. Note that in the IGD mode, despite having two-thirds the number of switching events compared to the $S = 1$ mode, a significant portion of these events occur under much higher electric fields (>45 kV/cm), where nonadiabatic transitions are extremely unlikely to occur. Excluding these high-field switching events, the nonadiabatic losses associated with the remaining switching events in the IGD mode are reduced to approximately half of those in the $S = 1$ mode. Furthermore, nonadiabatic transitions between states are predominantly relevant during low-phase-angle operations of the decelerator [57]. Conversely, the IGD and $S = 3$ operational modes generally utilize higher phase angles compared to the $S = 1$ mode to attain equivalent deceleration forces.

V. CONCLUSION

We introduced a deceleration strategy that efficiently reduces molecular losses in conventional pulsed Stark decelerators. The properties of the new operation mode, IGD, were theoretically analyzed. An experimental demonstration

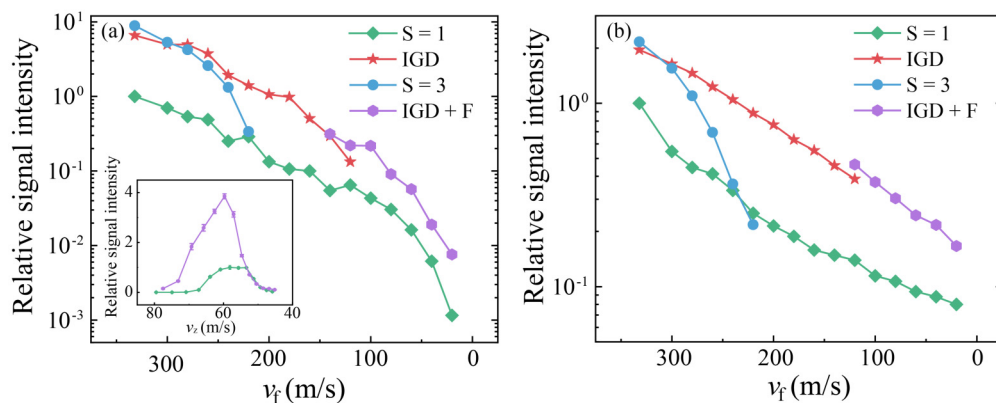


FIG. 6. (a) Observed molecular signal intensity of different operation modes over a range of final velocities. Data are collected with a beam of ND_3 at an initial speed of 332 m/s to 20 m/s. All data is normalized to the signal peak obtained in $S = 1$ operation mode at $\varphi_0 = 0^\circ$. The inset shows the decelerated packets with mean velocity of 60 m/s, utilizing IGD+F (purple) and $S = 1$ (green), respectively. The two lines normalized to the signal peak obtained in $S = 1$ operation mode. (b) Numerically calculated signal intensities for various operation modes over a range of final velocities. Note the logarithmic scale on the vertical axis.

was provided, revealing a significant advantage of the IGD over the standard $S = 1$ mode across high and intermediate final velocities (>100 m/s for ND_3 molecules). When combined with other methods, such as IGD + F, the decelerator achieves optimized deceleration efficiency for low final velocities (≤ 100 m/s for ND_3 molecules). While existing methods have successfully mitigated coherent loss mechanisms, they often necessitate either high-performance switching systems [41], additional calculations [45], or increased voltages [42]. In contrast, our method notably reduces wear on high-voltage switches, enhances system stability, and is readily scalable to manage multiple deceleration modules. It can be effortlessly incorporated into current experimental setups, presenting a cost-effective, efficient, and highly viable solution for most laboratory settings, thereby offering researchers an economical and potent alternative.

It is important to note that while the IGD mode identified here operates by guiding only every third instance, other operation modes such as every fifth or seventh guiding mode are also possible, facilitating the use of more electrodes for energy

removal. Additionally, by integrating our method with the focusing operation [42] at low final velocities, we can further enhance the number of molecules and the number density. Our method enables stopping a broader spectrum of molecular species with high density, including less favorable molecules with a small stark shift-to-mass ratio. It is expected to serve as an ideal tool for producing cold and dense molecular samples, offering further opportunities for fundamental and applied science such as precision measurement, cold collision, and quantum computation.

ACKNOWLEDGMENTS

This work is supported by the National Natural Science Foundation of China (Grants No. 91536218, No. 11874151, and No. 11834003), the Fundamental Research Funds for the Central Universities, the Program for Professor of Special Appointment (Eastern Scholar) at Shanghai Institutions of Higher Learning, and the Xinjiang Tianchi Talent Program (2023).

-
- [1] F. A. Gianturco and M. Tacconi, Concluding remarks: Achievements and challenges in cold and ultracold molecules, *Faraday Discuss.* **142**, 463 (2009).
- [2] S. Y. T. v. d. Meerakker and G. Meijer, Collision experiments with Stark-decelerated beams, *Faraday Discuss.* **142**, 113 (2009).
- [3] M. Kirste, X. Wang, H. C. Schewe, G. Meijer, K. Liu, A. van der Avoird, L. M. C. Janssen, K. B. Gubbels, G. C. Groenenboom, and S. Y. T. van de Meerakker, Quantum-state resolved bimolecular collisions of velocity-controlled OH with NO Radicals, *Science* **338**, 1060 (2012).
- [4] A. von Zastrow, J. Onvlee, S. N. Vogels, G. C. Groenenboom, A. van der Avoird, and S. Y. T. van de Meerakker, State-resolved diffraction oscillations imaged for inelastic collisions of NO radicals with He, Ne and Ar, *Nat. Chem.* **6**, 216 (2014).
- [5] J. J. Hudson, B. E. Sauer, M. R. Tarbutt, and E. A. Hinds, Measurement of the electron electric dipole moment using YbF molecules, *Phys. Rev. Lett.* **89**, 023003 (2002).
- [6] J. van Veldhoven, J. Küpper, H. L. Bethlem, B. Sartakov, A. J. A. van Roij, and G. Meijer, Decelerated molecular beams for high-resolution spectroscopy, *Eur. Phys. J. D* **31**, 337 (2004).
- [7] E. R. Hudson, H. J. Lewandowski, B. C. Sawyer, and J. Ye, Cold molecule spectroscopy for constraining the evolution of the fine structure constant, *Phys. Rev. Lett.* **96**, 143004 (2006).
- [8] W. Gerlach and O. Stern, Experimental proof of the magnetic moment of the silver atom, *Z. Phys.* **8**, 110 (1922).
- [9] H. L. Bethlem, G. Berden, and G. Meijer, Decelerating neutral dipolar molecules, *Phys. Rev. Lett.* **83**, 1558 (1999).
- [10] E. Vliegen, H. J. Wörner, T. P. Softley, and F. Merkt, Non-hydrogenic effects in the deceleration of Rydberg atoms in inhomogeneous electric fields, *Phys. Rev. Lett.* **92**, 033005 (2004).
- [11] E. S. Shuman, J. F. Barry, and D. DeMille, Laser cooling of a diatomic molecule, *Nature (London)* **467**, 820 (2010).
- [12] V. Zhelyazkova, A. Cournol, T. E. Wall, A. Matsushima, J. J. Hudson, E. A. Hinds, M. R. Tarbutt, and B. E. Sauer, Laser cooling and slowing of CaF molecules, *Phys. Rev. A* **89**, 053416 (2014).
- [13] J. D. Weinstein, R. deCarvalho, T. Guillet, B. Friedrich, and J. M. Doyle, Magnetic trapping of calcium monohydride molecules at millikelvin temperatures, *Nature (London)* **395**, 148 (1998).
- [14] R. deCarvalho, J. M. Doyle, B. Friedrich, T. Guillet, J. Kim, D. Patterson, and J. D. Weinstein, Buffer-gas loaded magnetic traps for atoms and molecules: A primer, *Eur. Phys. J. D* **7**, 289 (1999).
- [15] N. Vanhaecke, U. Meier, M. Andrist, B. H. Meier, and F. Merkt, Multistage Zeeman deceleration of hydrogen atoms, *Phys. Rev. A* **75**, 031402(R) (2007).
- [16] E. Narevicius, A. Libson, C. G. Parthey, I. Chavez, J. Narevicius, U. Even, and M. G. Raizen, Stopping supersonic beams with a series of pulsed electromagnetic coils: An atomic coilgun, *Phys. Rev. Lett.* **100**, 093003 (2008).
- [17] H. L. Bethlem, G. Berden, F. M. Cropvoets, R. T. Jongma, A. J. van Roij, and G. Meijer, Electrostatic trapping of ammonia molecules, *Nature (London)* **406**, 491 (2000).
- [18] S. Y. T. van de Meerakker, R. T. Jongma, H. L. Bethlem, and G. Meijer, Accumulating NH radicals in a magnetic trap, *Phys. Rev. A* **64**, 041401(R) (2001).
- [19] J. van Veldhoven, H. L. Bethlem, and G. Meijer, ac electric trap for ground-state molecules, *Phys. Rev. Lett.* **94**, 083001 (2005).
- [20] J. van Veldhoven, H. L. Bethlem, M. Schnell, and G. Meijer, Versatile electrostatic trap, *Phys. Rev. A* **73**, 063408 (2006).
- [21] S. Hoekstra, M. Metsälä, P. C. Zieger, L. Scharfenberg, J. J. Gilijamse, G. Meijer, and S. Y. T. van de Meerakker, Electrostatic trapping of metastable NH molecules, *Phys. Rev. A* **76**, 063408 (2007).
- [22] F. M. Cropvoets, H. L. Bethlem, R. T. Jongma, and G. Meijer, A prototype storage ring for neutral molecules, *Nature (London)* **411**, 174 (2001).
- [23] P. C. Zieger, S. Y. van de Meerakker, C. E. Heiner, H. L. Bethlem, A. J. van Roij, and G. Meijer, Multiple packets of

- neutral molecules revolving for over a mile, *Phys. Rev. Lett.* **105**, 173001 (2010).
- [24] C. E. Heiner, D. Carty, G. Meijer, and H. L. Bethlem, A molecular synchrotron, *Nat. Phys.* **3**, 115 (2007).
- [25] E. R. Hudson, C. Ticknor, B. C. Sawyer, C. A. Taatjes, H. J. Lewandowski, J. R. Bochinski, J. L. Bohn, and J. Ye, Production of cold formaldehyde molecules for study and control of chemical reaction dynamics with hydroxyl radicals, *Phys. Rev. A* **73**, 063404 (2006).
- [26] S. Y. van de Meerakker, H. L. Bethlem, N. Vanhaecke, and G. Meijer, Manipulation and control of molecular beams, *Chem. Rev.* **112**, 4828 (2012).
- [27] O. Bucicov, M. Nowak, S. Jung, G. Meijer, E. Tiemann, and C. Lisdat, Cold SO₂ molecules by stark deceleration, *Eur. Phys. J. D* **46**, 463 (2008).
- [28] B. L. Lev, E. R. Meyer, E. R. Hudson, B. C. Sawyer, J. L. Bohn, and J. Ye, OH hyperfine ground state: From precision measurement to molecular qubits, *Phys. Rev. A* **74**, 061402(R) (2006).
- [29] A. Fast, J. E. Furneaux, and S. A. Meek, Precision spectra of A²Σ⁺, v' = 0 ← X²Π_{3/2}, v'' = 0, J' = 3/2 transitions in ¹⁶OH and ¹⁶OD, *Phys. Rev. A* **98**, 052511 (2018).
- [30] B. C. Sawyer, B. K. Stuhl, M. Yeo, T. V. Tscherbul, M. T. Hummon, Y. Xia, J. Klos, D. Patterson, J. M. Doyle, and J. Ye, Cold heteromolecular dipolar collisions, *Phys. Chem. Chem. Phys.* **13**, 19059 (2011).
- [31] Z. Gao, T. Karman, S. N. Vogels, M. Besemer, A. van der Avoird, G. C. Groenenboom, and S. Y. T. van de Meerakker, Observation of correlated excitations in bimolecular collisions, *Nat. Chem.* **10**, 469 (2018).
- [32] D. DeMille, Quantum computation with trapped polar molecules, *Phys. Rev. Lett.* **88**, 067901 (2002).
- [33] S. F. Yelin, K. Kirby, and R. Côté, Schemes for robust quantum computation with polar molecules, *Phys. Rev. A* **74**, 050301(R) (2006).
- [34] B. C. Sawyer, B. K. Stuhl, B. L. Lev, J. Ye, and E. R. Hudson, Mitigation of loss within a molecular Stark decelerator, *Eur. Phys. J. D* **48**, 197 (2008).
- [35] S. Y. T. van de Meerakker, N. Vanhaecke, H. L. Bethlem, and G. Meijer, Transverse stability in a Stark decelerator, *Phys. Rev. A* **73**, 023401 (2006).
- [36] U. Even, The Even-Lavie valve as a source for high intensity supersonic beam, *EPJ Tech. Instrum.* **2**, 17 (2015).
- [37] H. Wu, D. Reens, T. Langen, Y. Shagam, D. Fontecha, and J. Ye, Enhancing radical molecular beams by skimmer cooling, *Phys. Chem. Chem. Phys.* **20**, 11615 (2018).
- [38] Y. Segev, N. Bibelnik, N. Akerman, Y. Shagam, A. Luski, M. Karpov, J. Narevicius, and E. Narevicius, Molecular beam brightening by shock-wave suppression, *Sci. Adv.* **3**, e1602258 (2017).
- [39] L. Scharfenberg, H. Haak, G. Meijer, and S. Y. T. van de Meerakker, Operation of a Stark decelerator with optimum acceptance, *Phys. Rev. A* **79**, 023410 (2009).
- [40] S. Y. T. van de Meerakker, N. Vanhaecke, H. L. Bethlem, and G. Meijer, Higher-order resonances in a Stark decelerator, *Phys. Rev. A* **71**, 053409 (2005).
- [41] D. Zhang, G. Meijer, and N. Vanhaecke, Advanced switching schemes in a Stark decelerator, *Phys. Rev. A* **93**, 023408 (2016).
- [42] D. Reens, H. Wu, A. Aeppli, A. McAuliffe, P. Wcisło, T. Langen, and J. Ye, Beyond the limits of conventional Stark deceleration, *Phys. Rev. Res.* **2**, 033095 (2020).
- [43] S. Hou, S. Li, L. Deng, and J. Yin, Dependences of slowing results on both decelerator parameters and the new operating mode: Taking ND₃ molecules as an example, *J. Phys. B* **46**, 045301 (2013).
- [44] L. P. Parazzoli, N. Fitch, D. S. Lobser, and H. J. Lewandowski, High-energy-resolution molecular beams for cold collision studies, *New J. Phys.* **11**, 055031 (2009).
- [45] J. J. Gilijamse, J. Küpper, S. Hoekstra, N. Vanhaecke, S. Y. T. van de Meerakker, and G. Meijer, Optimizing the Stark-decelerator beamline for the trapping of cold molecules using evolutionary strategies, *Phys. Rev. A* **73**, 063410 (2006).
- [46] M. Du, D. Zhang, and D. Ding, An alternative operation scheme to improve the efficiency of a Stark decelerator, *Chin. Phys. Lett.* **38**, 123201 (2021).
- [47] S. Hou, Q. Wang, L. Deng, and J. Yin, A switched ring Stark decelerator for both light and heavy polar molecules, *J. Phys. B* **49**, 065301 (2016).
- [48] Y. Shyur, J. A. Bossert, and H. Lewandowski, Pulsed operation of a ring Stark decelerator, *J. Phys. B At. Mol. Opt. Phys.* **51**, 165101 (2018).
- [49] A. Osterwalder, S. A. Meek, G. Hammer, H. Haak, and G. Meijer, Deceleration of neutral molecules in macroscopic traveling traps, *Phys. Rev. A* **81**, 051401(R) (2010).
- [50] M. I. Fabrikant, T. Li, N. J. Fitch, N. Farrow, J. D. Weinstein, and H. J. Lewandowski, Method for traveling-wave deceleration of buffer-gas beams of CH, *Phys. Rev. A* **90**, 033418 (2014).
- [51] J. E. van den Berg, S. C. Mathavan, C. Meinema, J. Nauta, T. H. Nijbroek, K. Jungmann, H. L. Bethlem, and S. Hoekstra, Traveling-wave deceleration of SrF molecules, *J. Mol. Spectrosc.* **300**, 22 (2014).
- [52] P. Aggarwal, Y. Yin, K. Esajas, H. L. Bethlem, A. Boeschoten, A. Borschevsky, S. Hoekstra, K. Jungmann, V. R. Marshall, T. B. Meijknecht *et al.*, Deceleration and trapping of SrF molecules, *Phys. Rev. Lett.* **127**, 173201 (2021).
- [53] S. A. Meek, M. F. Parsons, G. Heyne, V. Platschkowski, H. Haak, G. Meijer, and A. Osterwalder, A traveling wave decelerator for neutral polar molecules, *Rev. Sci. Instrum.* **82**, 093108 (2011).
- [54] S. C. Mathavan, A. Zapara, Q. Esajas, and S. Hoekstra, Deceleration of a supersonic beam of SrF molecules to 120 ms⁻¹, *ChemPhysChem* **17**, 3709 (2016).
- [55] N. E. Bulleid, R. J. Hendricks, E. A. Hinds, S. A. Meek, G. Meijer, A. Osterwalder, and M. R. Tarbutt, Traveling-wave deceleration of heavy polar molecules in low-field-seeking states, *Phys. Rev. A* **86**, 021404(R) (2012).
- [56] B. Wei, S. Y. Hou, H. Guo, Y. B. Ji, S. Q. Li, and J. P. Yin, Generation of high-energy-resolved NH₃ molecular beam by a Stark decelerator with 179 stages, *Chin. Phys. B* **28**, 053701 (2019).
- [57] T. E. Wall, S. K. Tokunaga, E. A. Hinds, and M. R. Tarbutt, Nonadiabatic transitions in a Stark decelerator, *Phys. Rev. A* **81**, 033414 (2010).